The Journal of Experimental Biology **199**, 281–294 (1996)
Printed in Great Britain © The Company of Biologists Limited 1996
JEB9963

AERODYNAMIC CHARACTERISTICS OF THE WINGS AND BODY OF A DRAGONFLY

MASATO OKAMOTO[1], KUNIO YASUDA[2] AND AKIRA AZUMA[3,*]

[1]*Wakayama Technical High School, Wakayama, Japan,* [2]*Department of Aerospace Engineering, College of Science and Technology, Nihon University, Funabashi, Japan* and [3]*University of Tokyo, 37-3 Miyako-cho, Saiwai-ku, Kawasaki 210, Japan*

Accepted 6 October 1995

Summary

The aerodynamic characteristics of the wings and body of a dragonfly and of artificial wing models were studied by conducting two types of wind-tunnel tests and a number of free-flight tests of gliders made using dragonfly wings. The results were consistent between these different tests. The effects of camber, thickness, sharpness of the leading edge and surface roughness on the aerodynamic characteristics of the wings were characterized in the flow field with Reynolds numbers (*Re*) as low as 10^3 to 10^4.

Key words: aerodynamics, dragonfly, wing, wind-tunnel test, gliding test, autorotational flight test, *Anax parthenope julius.*

Introduction

Wings of insects and samaras are small in size (with chord length c of the order of 1 cm or less) and used to fly at low speeds (speed V of the order of a few metres per second). This means that their wings operate in relatively more 'sticky' air than the wings of an aircraft or operate at low Reynolds numbers of 10^3 to 10^4 ($Re=Vc/\nu$, where ν is the kinematic viscosity of air). The aerodynamic characteristics of such wings at low Reynolds numbers have not been analyzed theoretically but have been studied experimentally (Weis-Fogh, 1956; Newman *et al.* 1977; Azuma and Okuno, 1987; Azuma and Watanabe, 1988; Azuma and Yasuda, 1989).

Three methods were used in the present study to investigate the aerofoil characteristics of dragonfly wings and model wings: (i) force and moment measurements in a horizontal wind-tunnel, (ii) autorotational flights in a vertical wind-tunnel, and (iii) gliding flights in still air.

The first method has been widely used previously (Pankhurst and Holder, 1952; Pope and Harper, 1966) and it is thus unnecessary to explain it in detail here. To succeed using this method, it is important to obtain a steady laminar airflow with a speed of less than $10\,m\,s^{-1}$ and to construct a balance system sensitive enough to measure small forces of the order of 10^{-4} N.

The second method was initially used by Azuma and Yasuda (1989) to analyze the aerodynamic characteristics of the samara aerofoil and was further developed to be applied to insect wings.

The third method is also commonly used to study the aerodynamic and flight dynamic characteristics of wing and wing–body combinations of flying devices operating at high Reynolds numbers. Azuma and Okuno (1987) and Azuma and Watanabe (1988) applied this method to a study of the lift and drag characteristics of samara wings and dragonfly wings, respectively, both of which operate at low Reynolds numbers.

Materials and methods

A horizontal wind-tunnel and its balance system

A horizontal wind-tunnel was constructed as shown in Fig. 1. The tunnel structure was made of wood, and the ceiling and one of the side walls of the test section were glass plates. The contraction ratio S_s/S_t between the area of the settling chamber S_s and the area of the test section S_t was 5.7. The wind speed was regulated by changing the rotational speed of a fan driven by a 200 W a.c. motor.

Temperature and atmospheric pressure were measured using a thermometer and an aneroid barometer, respectively. Wind speed U can be measured using, for example, an anemometer (0.2 Hz response) and/or a thermocouple anemometer (13 kHz response). However, at low speeds, as used in the present study, more precise values can be determined by counting the frequency (n) of the Karman vortex street observed downstream of a fine circular cylinder (diameter d) as follows (Roshko, 1960):

$$U = nd/St\,, \tag{1}$$

where St is the Strouhal number, which can be given as a function of the Reynolds number ($Re=Ud/\nu$, in which U may be a roughly estimated value),

*Author for correspondence.

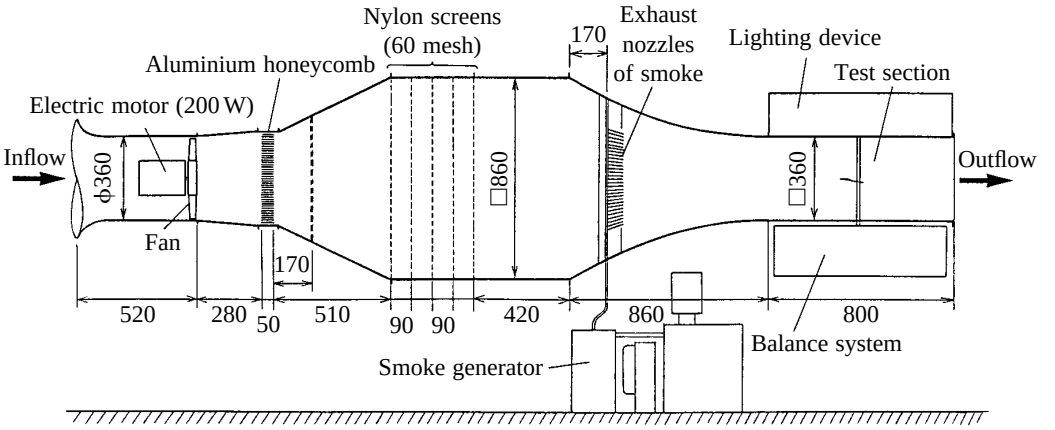

Fig. 1. Structure of the horizontal wind-tunnel. All dimensions are in millimetres. The tunnel structure was made of wood, and the ceiling and one side wall of the test section were glass plates. The wind speed was regulated by changing the rotational speed of a fan driven by a 200 W a.c. motor. The wind speed was usually $5\,m\,s^{-1}$ and the long-term speed variation (over several seconds) was within 1 %. For details of the balance system see Fig. 3. Symbols ϕ and □ show the diameter of the circular section and the length of the rectangular section, respectively.

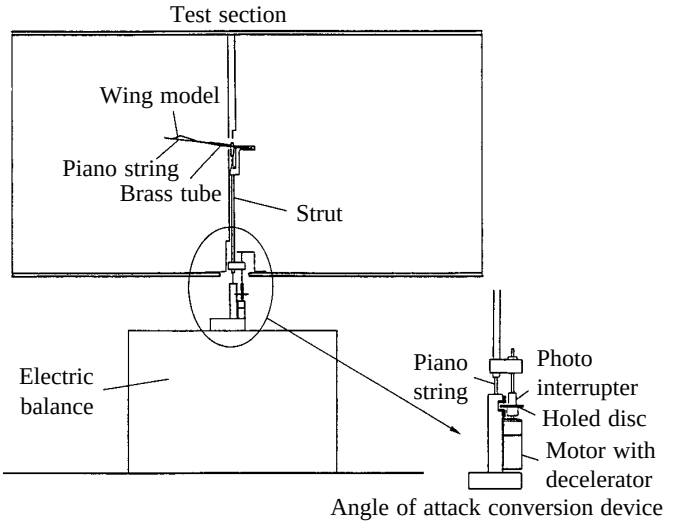

Fig. 2. The balance system used to measure forces from dragonfly wings and bodies in the wind-tunnel shown in Fig. 1. For details of the load cells used to measure the forces and contained in the electric balance system, see Fig. 3. The enlarged area shows the angle-of-attack conversion device in greater detail. For further details see text.

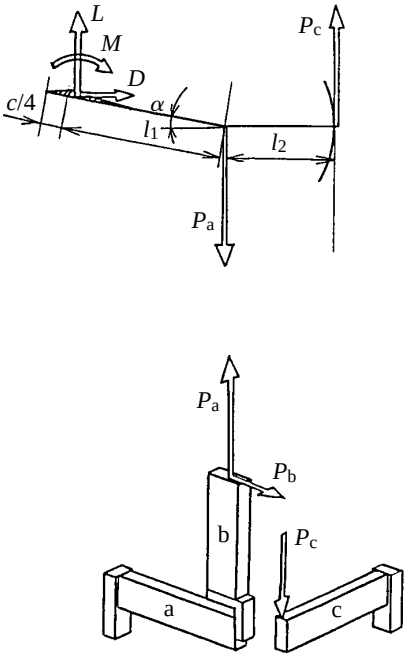

Fig. 3. Forces and moment derived for the load cells contained in the balance system. Load cells a, b and c are shown in the bottom panel. P_a, P_b and P_c are forces acting on load cells a, b and c, respectively, and α is the angle of attack of the setting support system. L, D and M are the lift, drag and moment acting along the direction of the arrows; l_1 and l_2 are the arm lengths of the acting point of forces; c is chord length.

$$St = 0.212(1 - 12.7/Re)\,. \qquad (2)$$

The wind speed was usually $5\,m\,s^{-1}$ and the long-term speed variation (over several seconds) was within 1 %. The turbulence intensity along the wind velocity $\sqrt{\overline{u^2}}$ (at frequencies greater then 10 Hz) was less than 0.3 % [$(\sqrt{\overline{u^2}}/U) < 0.3$ %].

For some tests, a lattice made of circular aluminium cylinders (4 mm diameter with 20 mm spacings) was arranged at the front of the test section to make the flow turbulent. This increased the turbulence intensity to 3.6 % for frequencies of 10 Hz to 2 kHz.

A balance system was constructed as shown in Fig. 2, using an A&D EK-120A-type electronic balance. The minimum measurable force was 10^{-4} N (or 10 mg). The sensors of the balance system consisted of three load cells constructed from aluminium alloy (load cells a and c measure lift and moment, and load cell b measures drag; see Fig. 3) with strain gauges attached to the plate surfaces of the load cells. The output data from strain gauges was processed by a personal computer (NEC PC-9801). The lift L, drag D and moment M were, as shown in Fig. 3, calculated as follows:

$$L = P_a - P_c\,, \qquad (3)$$

$$D = P_b\,, \qquad (4)$$

$$M = -l_1(L\cos\alpha + D\sin\alpha) + l_2 P_c\,, \qquad (5)$$

where P_a, P_b and P_c are forces acting on load cells a, b and c, respectively, l_1 and l_2 are the arm lengths of the acting point of the forces and α is the angle of attack of the setting support system (Fig. 3). Initial loads derived from gravity and the

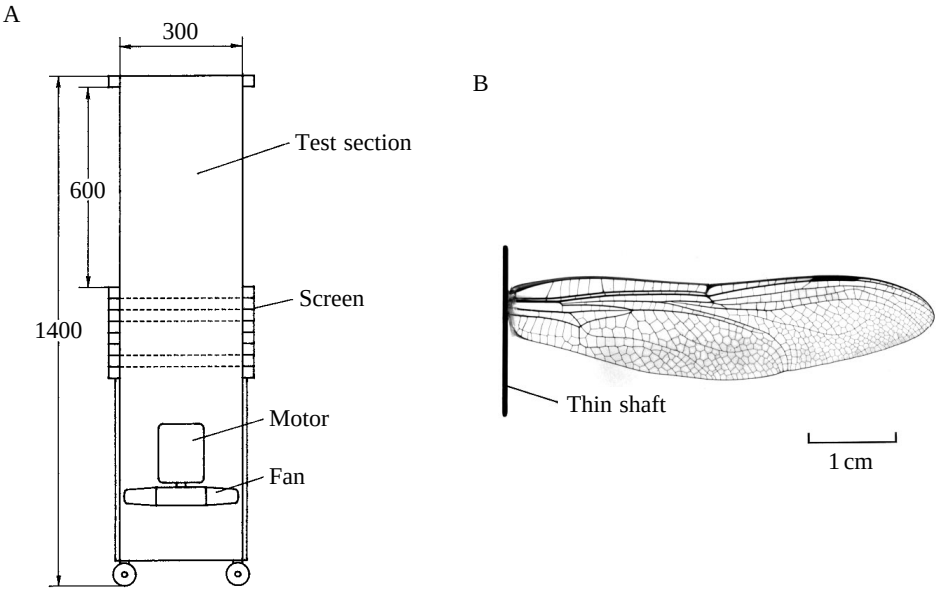

Fig. 4. (A) Structure of the vertical wind-tunnel. All dimensions are in millimetres. The upward flow of air is provided by a fan driven by a 0.75 kW a.c. motor. The cross-sectional area of the tunnel is 300 mm× 300 mm. (B) Dragonfly forewing modified for autorotational flight by attaching a thin fibreglass shaft to the wing root in order to alter the position of the centre of gravity as required.

aerodynamic forces acting on the wetted surface of the support system were subtracted from the measured values. The angle of attack α was altered automatically at a rate of approximately $0.4^{\circ}\,s^{-1}$ by the electric motor of the angle of attack conversion device shown in Fig. 2. At 0.36° intervals, the conversion device was stopped momentarily for about 1 s to record force and moment data. The sweeping speed ($0.4^{\circ}\,s^{-1}$) is so low and the stopped duration during the measurements is relatively so long that any unsteady effects on the aerodynamic characteristics of the wings may be neglected. Mean force and moment data were recorded 10 times during each 1 s period for which the conversion device was stopped. The aerodynamic coefficients (lift coefficient, C_L; drag coefficient C_D and moment coefficient C_M) were obtained as a function of angle of attack α as follows:

$$C_L = L/0.5\rho V^2 S, \quad (6)$$

$$C_D = D/0.5\rho V^2 S, \quad (7)$$

$$C_M = M/0.5\rho V^2 Sc, \quad (8)$$

where ρ is the air density, V is the flight speed (which, in the present case, is equal to the wind speed U) and S is the wing area.

In order to check the homogeneity of the flow in the wind-tunnel and the accuracy of the balance system, the drag of a sphere of diameter 38 mm was measured. For this sphere, C_D=0.43 at a Reynolds number of 1.16×10^4. This is in good agreement with a published value at the same Reynolds number (Hoerner, 1965).

Vertical wind-tunnel and autorotational flight of a dragonfly wing

A vertical wind-tunnel was constructed and arranged as shown in Fig. 4A. A fan driven by a 0.75 kW a.c. motor located below the screens provided the upward flow of air in the test section. The flow was damped by passing through damping screens made of stainless steel. The test section with a square cross section was constructed from four transparent acrylic plates.

It is possible to obtain a steady autorotational flight from a dragonfly wing by adjusting the position of the centre of gravity (Fig. 4B). By selecting a suitable wind speed in the tunnel, a spinning wing can be made to float in the test section. At this point, the wind speed measured by the anemometer is equal to the rate of descent of the spinning wing. The rotational speed Ω, the coning angle β_0 and the feathering angle θ can be measured using a stroboscopic flash synchronized with the spinning rate of the wing to 'freeze' the image, as described by Azuma and Yasuda (1989). The aerodynamic characteristics of the two-dimensional wing can be obtained from analysis of these data, as described below.

Gliding flight

If the centre of gravity of a wing is located in front of and near to the aerodynamic centre, it is possible for a wing to perform a gliding flight. As shown by Azuma and Okuno (1987), by taking a series of photographs of the steady gliding flight of a wing using a stroboscope, the flight speed of the wing V, the gliding angle γ and the angle of attack α can be measured. Fig. 5 shows representative photographs of the flight path of a dragonfly wing in steady gliding flight in side and front views. These experiments were carried out in still air.

By changing the longitudinal location of the centre of gravity, V, γ and α can be altered and the three-dimensional aerodynamic characteristics of the wing (C_L, C_D and C_M) can be determined as a function of angle of attack α.

Results and discussion

Wind-tunnel test results of model wings

The three-dimensional aerodynamic characteristics of model rectangular wings constructed from aluminium foil or balsa

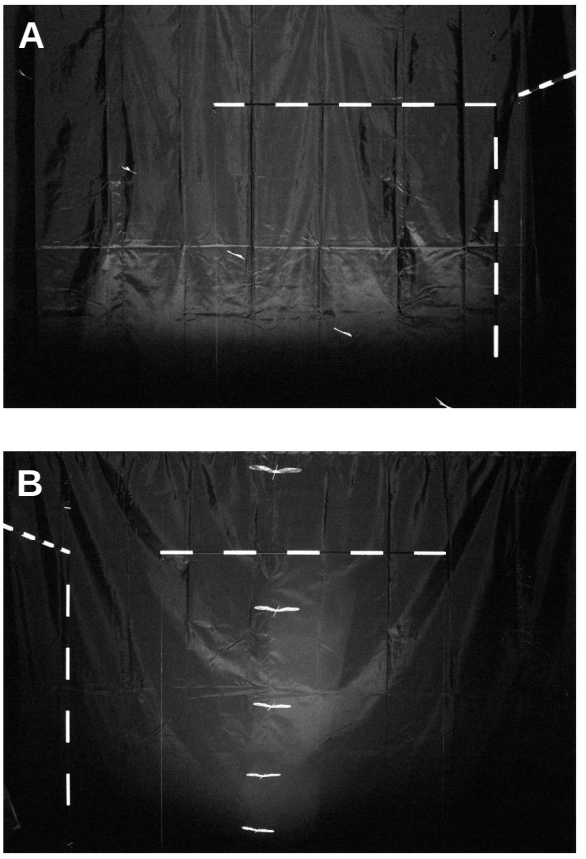

Fig. 5. Multiple-exposure photographs showing the free flight of a glider made from a pair of dragonfly wings. The centre of gravity of the wing was altered by changing the position of the thin shaft in order to obtain steady gliding flight. These tests were conducted in still air. (A) Flight path profile; (B) front view.

wood (aspect ratio AR=6), i.e. the lift and drag coefficients C_L and C_D, as a function of the angle of attack α and the polar curve were obtained at Reynolds numbers of 1.1×10^4 to 1.5×10^4 in the laminar flow of the horizontal wind-tunnel for models of different sizes, camber and shape.

Effects of plate thickness

The effects of flat plate thickness on the aerodynamic characteristics of the model wings are shown in Fig. 6. It can be seen that the thinner wings have a better performance with a smaller drag coefficient C_D and a larger maximum lift coefficient $C_{L,max}$. They also have a slightly lower lift curve slope $dC_L/d\alpha$.

Effects of camber

The effects of circular and triangular camber of the model wing on its aerodynamic characteristics are shown in Figs 7 and 8, respectively.

As the camber increases positively (upwardly convex), the maximum lift coefficient $C_{L,max}$, the minimum drag coefficient C_{D_0} and the lift curve slope $dC_L/d\alpha$ all increase. However, as the camber increases negatively (downwardly convex), the lift curve slope $dC_L/d\alpha$ and the minimum drag coefficient C_{D_0} increase, but the maximum lift coefficient $C_{L,max}$ clearly decreases.

As the chordwise location of the maximum camber of the triangular aerofoil moves backwards (see right-hand panel in Fig. 8), the aerodynamic characteristics of the model wing deteriorate slightly except for the slope of the lift curve.

It can be further observed that the slope of a tangential line from the origin to the respective polar curve, or the maximum lift-to-drag ratio $(L/D)_{max}$, has the largest value for the 3 %

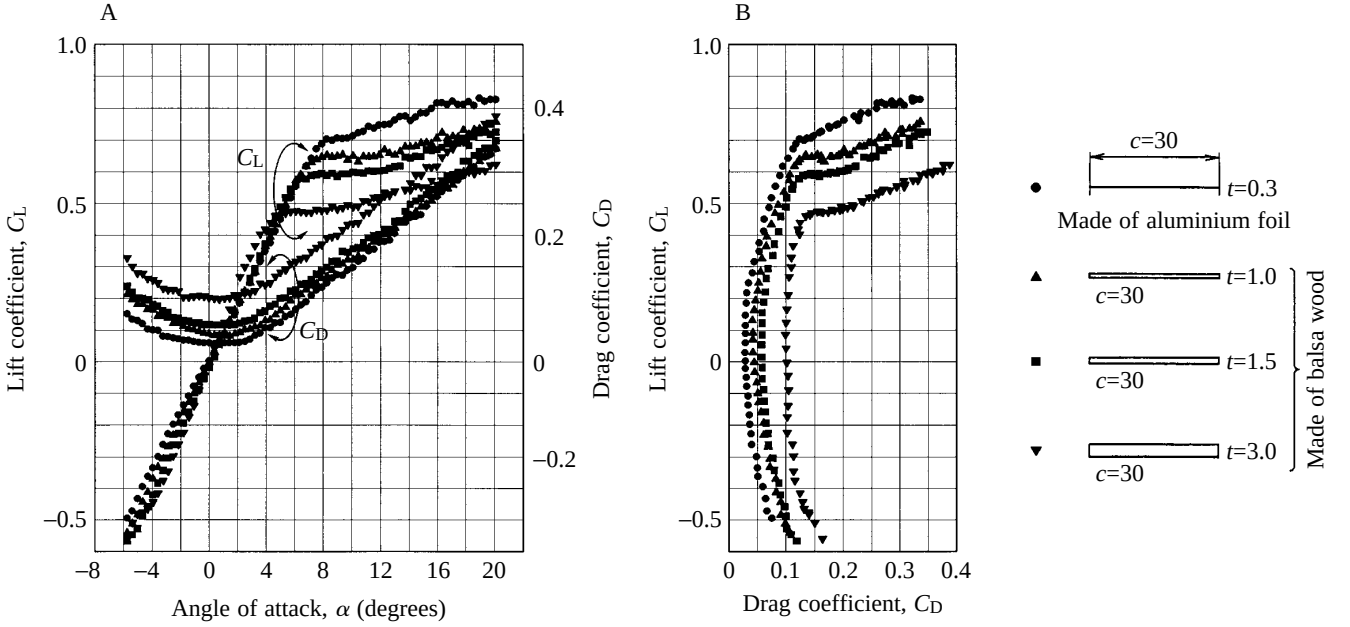

Fig. 6. Effects of the thickness of a flat plate on its aerodynamic characteristics. Each symbol refers to a different model, the shape of which is shown in the panel on the right of the figure; *t*, thickness, *c*, chord length. All measurements are given in millimetres. (A) C_L and C_D *versus* α. (B) Polar curve.

upwardly convex circular curve. Also, the lift coefficient at $(L/D)_{max}$, $C_{L,(L/D)max}$, is lower for the aerofoils with less camber.

Surface waviness

The effects of the surface contour of smooth and corrugated flat plate model wings on their aerodynamic characteristics are

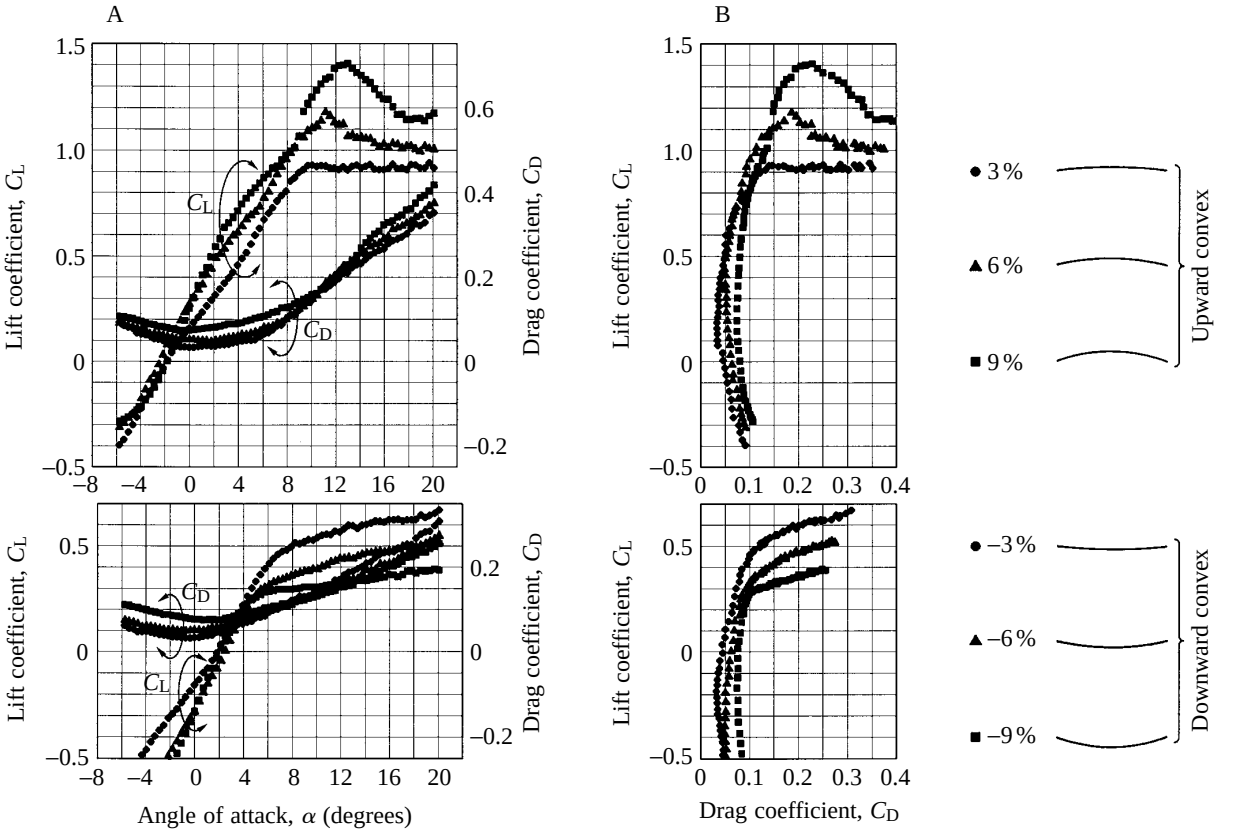

Fig. 7. Effects of circular camber on the aerodynamic characteristics of a rectangular model wing made from aluminium foil, thickness 0.3mm, chord length 30 mm. Each symbol refers to a different camber, as shown in the panel on the right of the figure. (A) C_L and C_D *versus* α. (B) Polar curve.

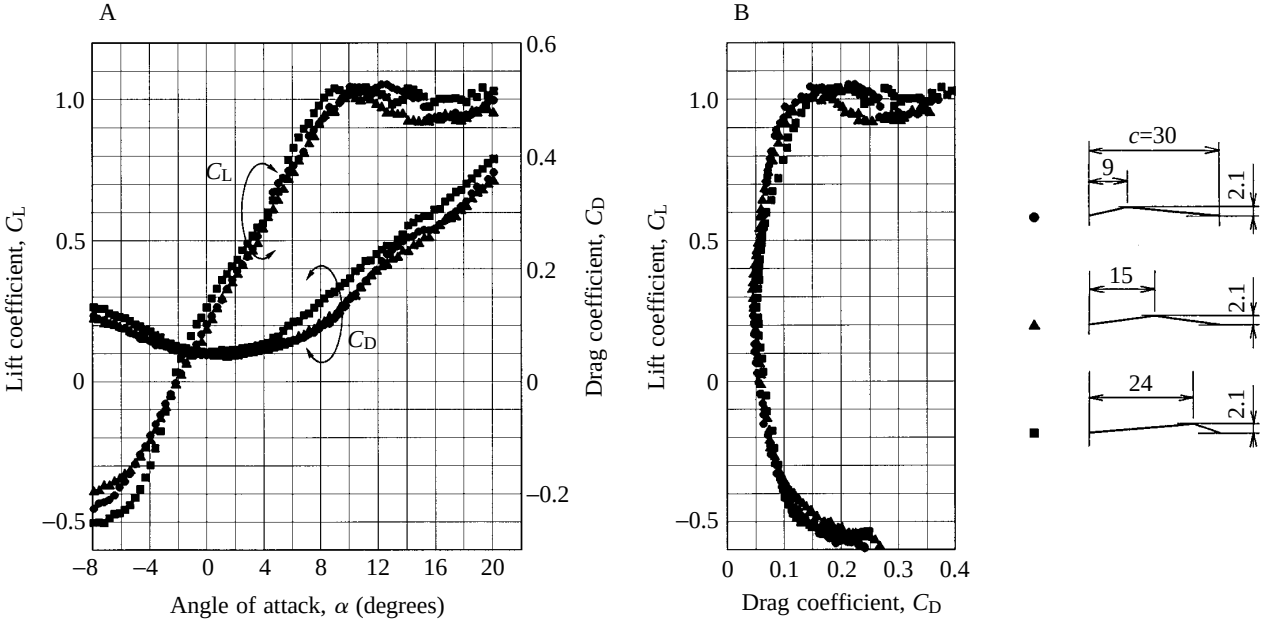

Fig. 8. Effects of triangular camber on the aerodynamic characteristics of a model wing constructed from aluminium foil, thickness 0.3 mm, chord length 30 mm. Each symbol refers to a different triangular camber (camber held constant at 7%) shown in the panel on the right of the figure; *c*, chord length. All dimensions are given in millimetres. (A) C_L and C_D *versus* α. (B) Polar curve.

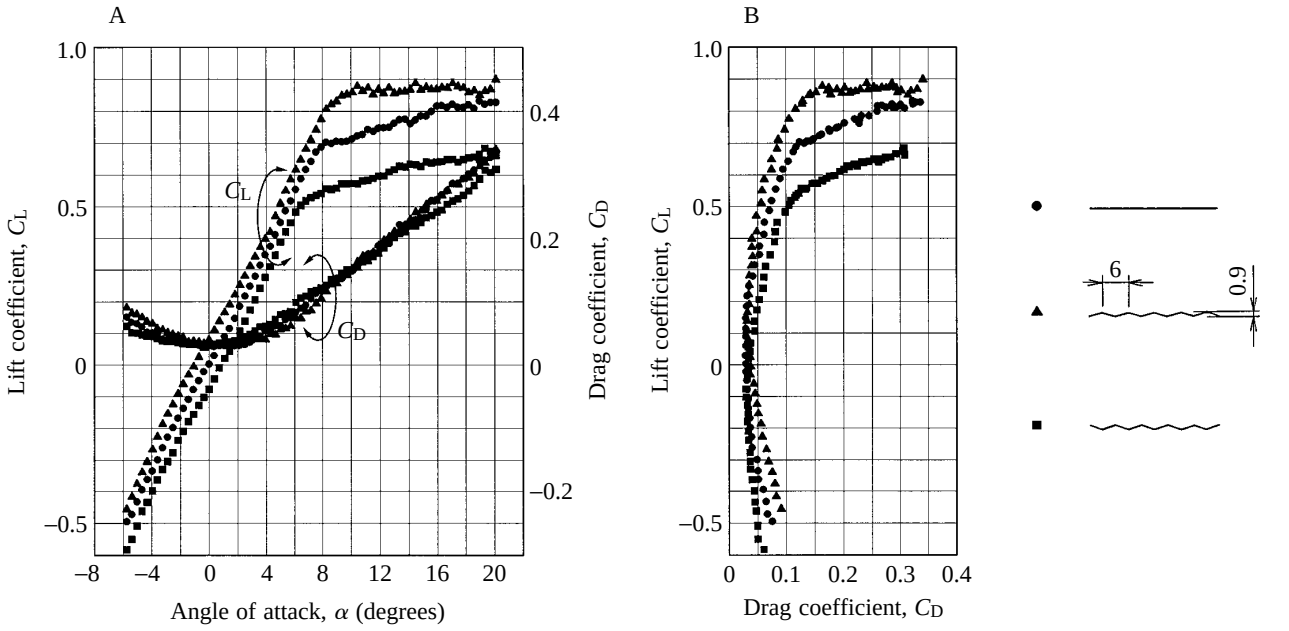

Fig. 9. Effects of surface contour on the aerodynamic characteristics of a model wing constructed from aluminium foil. Wing chord length 30 mm, thickness 0.3 mm. Each symbol refers to the wing shape shown in the panel on the right. Dimensions are given in millimetres. Note that the dimensions for the two corrugated wings are the same. These two models differ only in the configuration at the leading edge. (A) C_L and C_D *versus* α. (B) Polar curve.

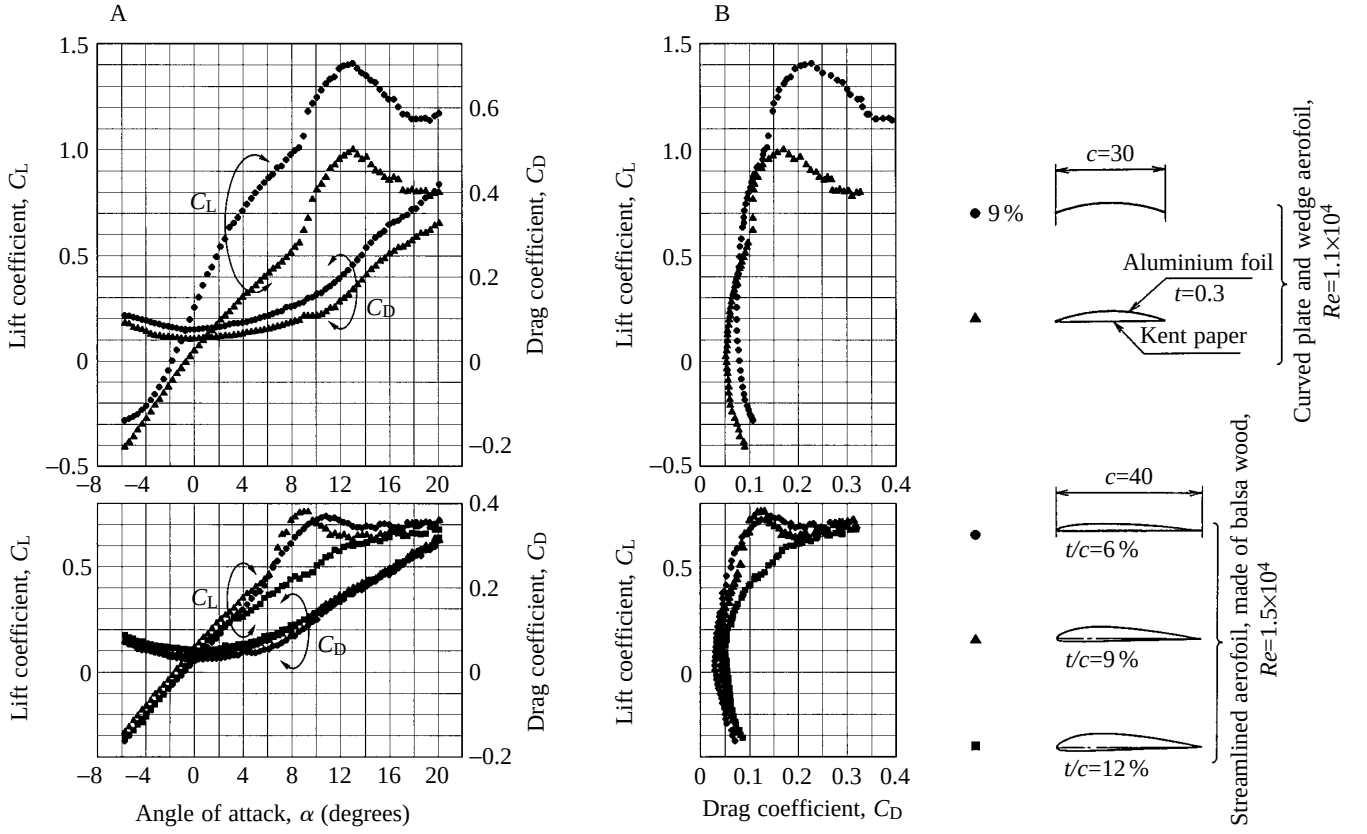

Fig. 10. Effects of thickness on the aerodynamic characteristics of a curved-section model wing (camber 9 %) constructed from aluminium foil and Kent paper or balsa wood as shown. Each symbol refers to a different aerofoil shape as shown in the panel on the right; *c*, chord length; *t*, thickness; *Re*, Reynolds number. All dimensions are given in millimetres. (A) C_L and C_D *versus* α. (B) Polar curve.

shown in Fig. 9. The surface contours scarcely affect the lift curve slope $dC_L/d\alpha$ and the minimum drag coefficient C_{D_0}, but the maximum lift coefficient $C_{L,max}$ and the drag coefficient C_D at large angles of attack are obviously altered. It is interesting that (i) the configuration at the leading edge seems to be important; the aerofoil with the downward-facing leading edge has a much better performance than the upward-facing model, (ii) increasing the surface roughness increases not only the maximum lift-to-drag ratio $(L/D)_{max}$ but also the lift coefficient at $(L/D)_{max}$, $C_{L,(L/D)max}$.

Effect of aerofoil thickness

The effects of the thickness of a curved-section model wing on its aerodynamic characteristics are shown in Fig. 10. Generally, as the thickness of the curved-section model wing increases, its aerodynamic characteristics deteriorate. It can be seen that the maximum lift coefficient $C_{L,max}$ is highest for the thin curved plate with a positive curvature of 9 %.

Leading-edge sharpness

The effects of leading-edge sharpness on the aerodynamic characteristics of model wings are clearly shown in Fig. 11. For the flat plate, a sharp leading edge was formed by tapering the upper surface, and for the aerofoil a thin plate was added to the lower surface so as to extend the chin (Fig. 11). The minimum drag coefficient C_{D_0} and the lift curve slope $dC_L/d\alpha$ are scarcely altered by these features but the maximum lift coefficient $C_{L,max}$ increased markedly with increasing leading-edge sharpness.

It can be concluded that increased leading-edge sharpness results in an increase in the maximum lift-to-drag ratio $(L/D)_{max}$ (which is represented by the tangential line from the origin to the polar curve) and also an increase in the lift coefficient at $(L/D)_{max}$, $C_{L,(L/D)max}$. This is very similar to the effects of increased surface roughness (Fig. 10).

Effect of turbulence

The effects of increased turbulence, caused by inserting a lattice of aluminium cylinders into the tunnel, on the aerodynamic characteristics of the model wings are clearly seen in Figs 12 and 13, for the thin plate and for the wing with an aerofoil section and a smooth surface, respectively. The difference between the aerodynamic characteristics tested in the laminar (<0.3 % turbulence) and turbulent (3.6 %) flows for the thin plate are not as great as they are for the model wing with an aerofoil section except for the lift slope values. For the flat plate, the lift slope is higher in the laminar flow than in the turbulent flow (Fig. 12A). However, for the aerofoil section (Fig. 13), there are large differences in C_L at high angles of attack. The wing with an aerofoil section and a smooth surface operating in turbulent flow exhibits a higher lift coefficient and a lower drag coefficient at a given angle of attack than the same wing operating in laminar flow, which can be considered to be a better performance.

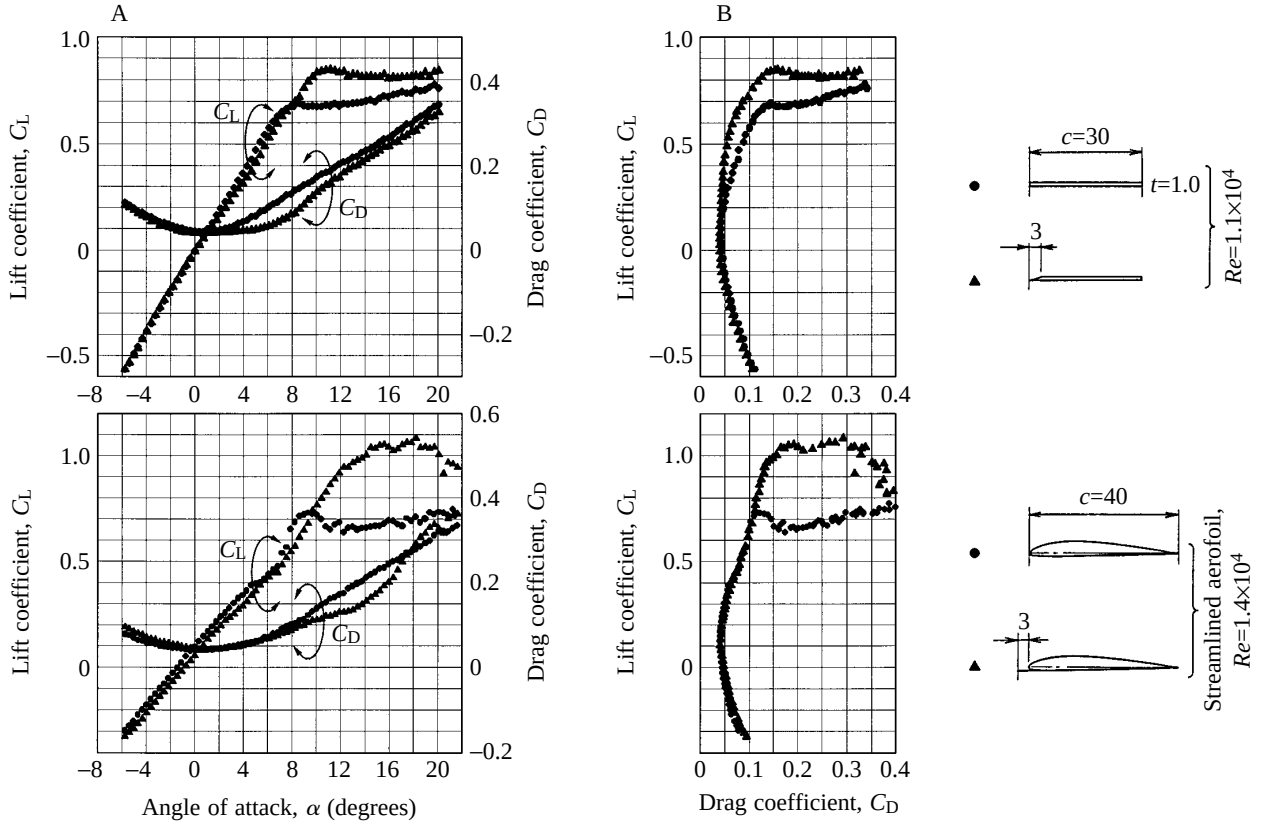

Fig. 11. Effects of leading-edge sharpness on the aerodynamic characteristics of model wings constructed from balsa wood. Each symbol refers to a different wing shape as shown on the right of the figure; *c*, chord length; *t*, thickness; *Re*, Reynolds number. All dimensions are given in millimetres. (A) C_L and C_D *versus* α. (B) Polar curve.

Dragonfly wings and body

The aerodynamic characteristics of a dragonfly, *Anax parthenope julius* (Brauer), were studied using the horizontal wind-tunnel. Autorotational tests in the vertical wind-tunnel and free-flight or gliding tests in still air were also conducted using models of dragonfly wings. Morphological measurements for two dragonflies are given in Tables 1 and 2. Fig. 14 shows examples of magnified cross sections of the wings of dragonfly A (see Table 1) photographed using a microscope. The sections were obtained by fixing the wings with resin and then slicing them transversely into several elements.

Wind-tunnel test

The first wind-tunnel tests were performed using a pair of fore- and hindwings. The right and left wings of the respective pair were connected using a steel wire (diameter 1 mm) as shown in Fig. 15A. However, because of the lack of stiffness in the wing, it twisted along its span and accurate measurements of the aerodynamic characteristics of the natural wing could not be made. During normal flights, this twisting of the wing must be adaptive (Azuma and Watanabe, 1988). In the later tests, therefore, a single wing was used, supported by a frame made of steel wire (as shown in Fig. 15B) to reduce twisting during the test. The aspect ratio of this single modified wing is half that of the paired wings.

The modified wings were tested in the horizontal wind-tunnel, and the results are shown in Fig. 16. The maximum lift coefficient $C_{L,max}$, which is close to 1.0, will depend not only on the geometrical characteristics of the wing cross section but also on the aspect ratio of the wing. The 9 % circular-cambered and triangular-cambered thin plates (Figs 7, 8), the flat corrugated plate (Fig. 9) and the wedge-shaped aerofoil

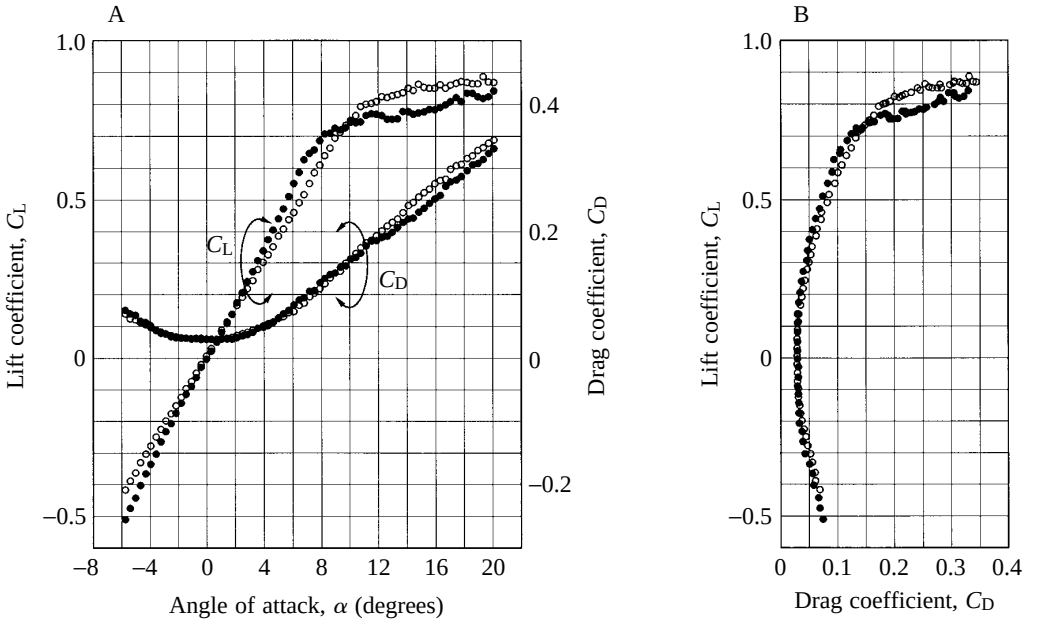

Fig. 12. Effects of turbulence on the aerodynamic characteristics of a thin plate, chord length 30 mm, thickness 0.3 mm. Filled circles indicate a turbulence level of less than 0.3 %, open circles a level of 3.6 %. (A) C_L and C_D *versus* α. (B) Polar curve.

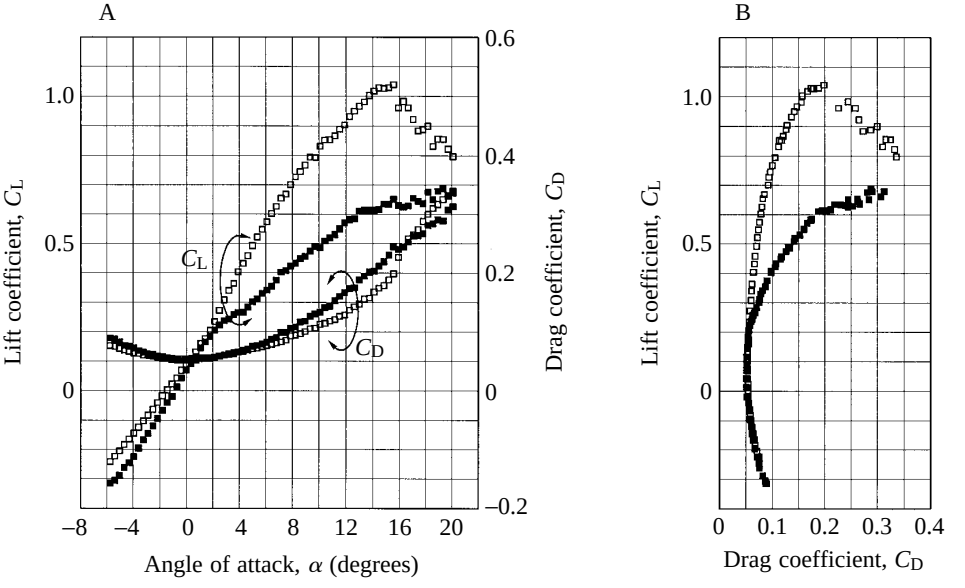

Fig. 13. Effects of turbulence on the aerodynamic characteristics of an aerofoil section, chord length 40 mm, thickness/chord length 12 %. Filled squares indicate a turbulence level of less than 0.3 %, open squares are for a level of 3.6 %. (A) C_L and C_D *versus* α. (B) Polar curve.

(Fig. 10) also had $C_{L,max}$ values close to 1.0, which is higher than that produced by streamlined aerofoils with a smooth surface and of various thicknesses. The minimum drag coefficient C_{D_0} is larger than that of the artificial aerofoils. This is probably a penalty incurred by increasing the stiffness of the wing using staggered or zigzag veins. However, as stated above, a rough or contoured surface is favourable for other aerodynamic characteristics.

Table 1. *Dimensional characteristics of two dragonflies*
Anax parthenope julius

	A	B
Body length, l_b (mm)	70.5	72.0
Maximum cross-sectional area of body, S_c (mm^2)	95	–
Wing span, b (mm)		
Forewings b_f	99.8	105.8
Hindwings b_h	101.8	103.8
Wing area, S (mm^2)		
Forewings S_f	890	960
Hindwings S_h	1100	1220
Aspect ratio, AR		
Forewings AR_f	11.19	11.66
Hindwings AR_h	9.42	8.83
Mean aerodynamic chord, $\bar{c}(=b/AR)$ (mm^2)		
Forewings $\bar{c}_f$	8.92	9.07
Hindwings $\bar{c}_h$	10.81	11.76
Mass, m_b (g)	0.79	0.79

Table 2. *Measurements for the autorotational flight of the right forewing of a dragonfly*

Mass, m_w (mg)	22.8
Wing area, S_f (mm^2)	502
Rate of descent, V (m s^{-1})	0.41
Autorotation speed, Ω (revs min^{-1})	550
Coning angle, β_0 (degrees)	45
Pitch angle, $\theta_{0.75}$ (degrees)	–1

Gliding and autorotational tests

Free or gliding flights were performed using four tailless gliders constructed from a pair of fore- or hindwings of a dragonfly as in Fig. 15A. However, without a tail, these gliders performed steady gliding flight only if the wings were inverted (upside-down), in which case the mean camber of the wings was convex downwards (Azuma and Okuno, 1987; Azuma, 1992). As stated above, the flight profiles of the gliders were photographed using a stroboscope and the pictures analyzed to obtain the polar curve of the wings.

Autorotational flight of the wings of a dragonfly in the vertical wind-tunnel was carried out for a small range of changes in the position of the centre of gravity of the wing (see Fig. 4B). The test apparatus and the methods used were those reported by Azuma and Yasuda (1989). Briefly, by (i) assuming homogeneous aerofoil characteristics along the wingspan such that:

$$C_l = a(\alpha - \alpha_{C_l=0}) \text{ for the range } C_l < C_{l,max}, \quad (9)$$

$$C_l = C_{l,max} \text{ for the range } C_l \geqslant C_{l,max}, \quad (10)$$

$$C_d = C_{d_0} + C_{d,\alpha}\alpha + C_{d,\alpha^2}\alpha^2, \quad (11)$$

where the lift slope a, minimum drag coefficient C_{d_0} and the maximum lift coefficient $C_{l,max}$ of the two-dimensional model wing are unknown values, but the zero lift angle $\alpha_{C_l=0}$ and the drag derivatives $C_{d,\alpha}$ and C_{d,α^2} for the two-dimensional model wing are known values obtained from wind-tunnel tests and are given in Table 3; and (ii) by measuring the rotational speed Ω, wind speed (or vertical descent speed) V, and the coning angle of the rotating wing β_0, in the vertical wind-tunnel (results given in Table 2), and (iii) by applying the local circulation method (LCM; Azuma and Yasuda, 1989; Azuma, 1992) to analyze the aerofoil characteristics, the three unknown

Table 3. *Aerodynamic data obtained from the tests on dragonfly wings*

	Autorotational flight (Forewing)	Wind-tunnel and gliding flight tests		
		Forewing	Hindwing	Range of α
Lift slope, a (rad^{-1})	4.90	4.81	4.96	$\alpha > \alpha_{C_l=0}$
	–	3.33	2.43	$\alpha < \alpha_{C_l=0}$
Zero lift angle, $\alpha_{C_l=0}$ (rad)	0*	0	–2.72	$\alpha > \alpha_{C_l=0}$
	–	0	1.33	$\alpha < \alpha_{C_l=0}$
Minimum drag coefficient, C_{d_o}	0.060	0.0960	0.0881	$\alpha > \alpha_{C_l=0}$
	–	0.0964	0.0892	$\alpha < \alpha_{C_l=0}$
$C_{d,\alpha}$ (rad^{-1})	–0.0888*	–0.0888	0.1532	$\alpha > \alpha_{C_l=0}$
	–	–0.1240	0.2096	$\alpha < \alpha_{C_l=0}$
C_{d,α^2} (rad^{-2})	2.005*	2.005	1.900	$\alpha > \alpha_{C_l=0}$
	–	2.800	2.600	$\alpha < \alpha_{C_l=0}$
Maximum lift coefficient, $C_{l,max}$	0.90	0.97	1.01	$\alpha > \alpha_{C_l=0}$
	–	0.54	0.46	$\alpha < \alpha_{C_l=0}$

*Values used in autorotational test local circulation method calculations.
For further details, see text.

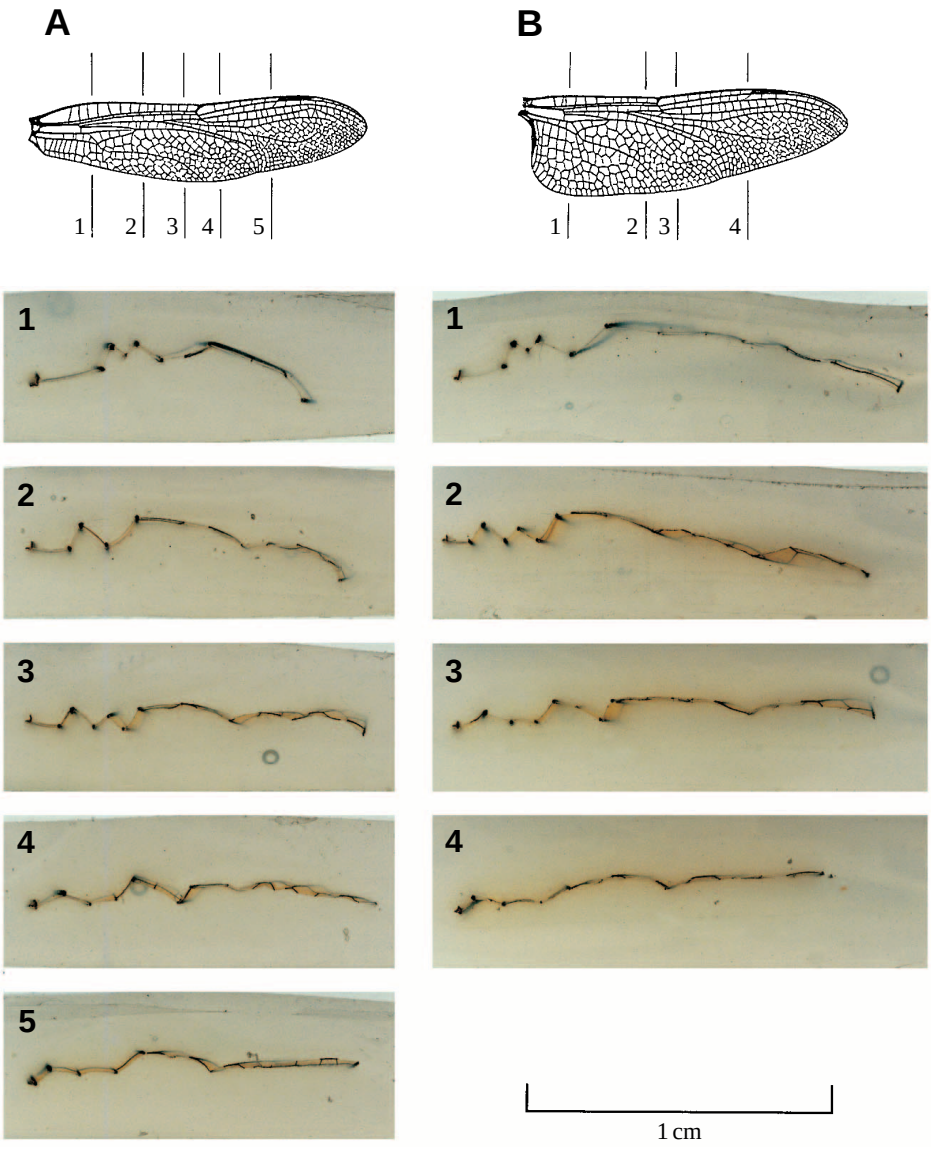

Fig. 14. Photographs of cross sections of the fore- and hindwing of a dragonfly taken through the positions shown in the diagrams at the top of the figure. (A) Forewing; (B) hindwing.

values a, C_{d_0} and $C_{l,max}$ can be obtained. The aerodynamic characteristics of the forewing of the dragonfly were obtained by using this approach with our data.

Test results

The aerodynamic characteristics of two-dimensional wings or aerofoils can be derived from those of three-dimensional wings by applying any wing theory (Anderson, 1933, 1936; Azuma and Okuno, 1987; Azuma, 1992) for the fixed wing and the LCM for the rotary wing.

The plots shown in Fig. 17 are from the glider constructed from both pairs of dragonfly wings (see Fig. 15A; AR=12) and also the modified single wing (see Fig. 15B; AR=6) obtained using the horizontal wind-tunnel test. Although the data for the gliding flight using the wings from individuals 1–4 were confined to negative lift coefficients (or negative angles of attack), the agreement between data from both tests is considered to be good. The solid curves in Fig. 17 show representative polar curves for the experimental data obtained using a three-dimensional wing, whereas the dashed curves show polar curves for two-dimensional wings calculated from the polar curves of the three-dimensional wings by applying the LCM.

As stated above, the angle of attack was altered at a rate of $0.4\,^{\circ}\,s^{-1}$ ($|\dot{\alpha}|=0.4\,^{\circ}\,s^{-1}$) and stopped for a duration of about 1 s. Thus, the rate of change of the angle of attack is considered to be small enough to avoid unsteady effects on the aerodynamic characteristics due to the angular motion because the non-dimensional rate of change of the angle of attack based on a chord length c of approximately 0.01 m and a wind speed U of $5\,m\,s^{-1}$ and where $|\alpha'|=|\dot{\alpha}|c/2U$, is of the order of 10^{-5} or less. This non-dimensional rate is so small in an aerodynamic sense that any unsteady effects on the forces and moments measured can be neglected (Bisplinghoff *et al.* 1957).

The wind-tunnel data shown in Fig. 17 showed a little hysteresis for the change of angle of attack [compare data for filled circles ($\dot{\alpha}>0$) and crosses ($\dot{\alpha}<0$)]. This hysteresis seems to be caused by the non-linear behaviour of the wing torsional

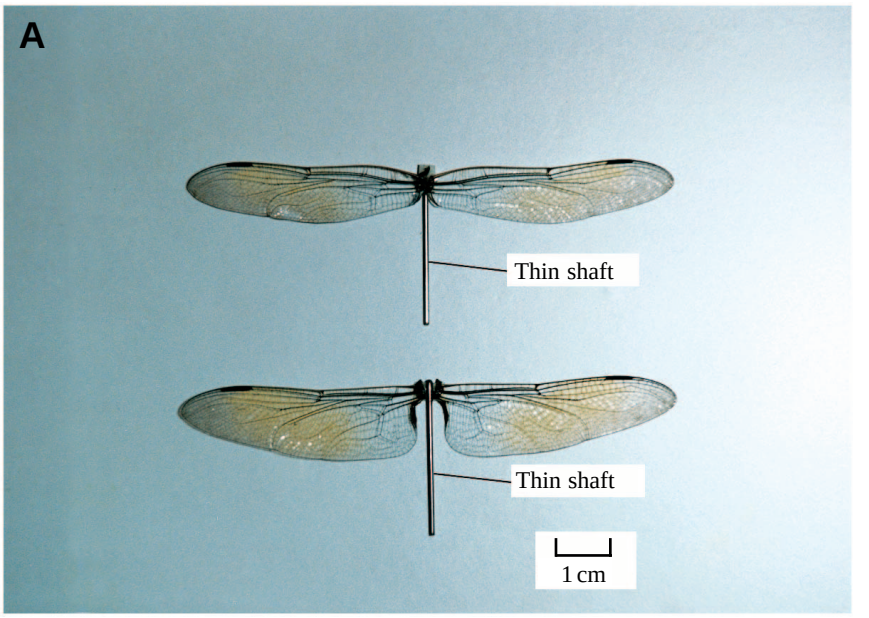

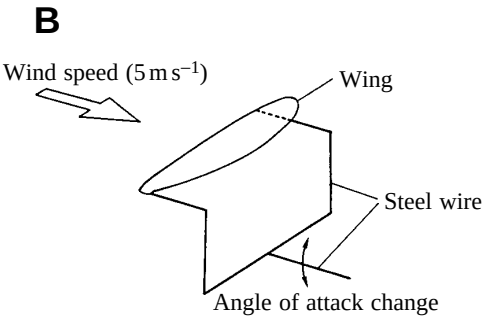

Fig. 15. (A) Forewings (upper pair) and hindwings (lower pair) of a dragonfly mounted either on steel wire as shown (diameter 1 mm) for use in the initial wind-tunnel tests (see text) or on balsa wood for the free-flight test. (B) Modified approach for later tests. A single wing, supported by a frame made of 1 mm diameter steel wire, was used to reduce wing twisting during measurements.

deformation, similar to the strength characteristics of plastic materials. This was, however, not confirmed in the flight test.

Fig. 18 gives the two-dimensional (or aerofoil) characteristics (C_l and C_d) of the forewing of a dragonfly calculated using the LCM from data from the three different experimental methods; the wind-tunnel tests, the gliding tests and the autorotational tests. The curves drawn with solid lines are calculated from the polar curves obtained in the horizontal wind-tunnel test and the gliding test, and thus correspond to the curves shown by the dashed lines in Fig. 17. The curves drawn with broken lines are obtained by the autorotational test in the vertical wind-tunnel. The results obtained using equations 9–11 on our data are given in Table 3.

It can be seen that the lift curve slopes are in excellent agreement between the two experimental approaches, but there are slight discrepancies in values for the maximum lift coefficient and the minimum drag coefficient. These discrepancies are probably due to the fact that the two-dimensional aerodynamic characteristics are mean values of spanwise functions of a three-dimensional wing. For gliding flight, the aerodynamic characteristics near the wing root are treated equally to those near the wing tip. However, in the autorotational flight, the aerodynamic characteristics near the wing tip are more emphasized than those near the wing root because of the lower airspeed near the wing root. Thus, the broken curves may be considered to represent the two-dimensional aerodynamic characteristics near the wing tip.

The drag and lift coefficients of the body of dragonfly A (Table 1) are given from the wind-tunnel test at a Reynolds number of 2.4×10^4 (based on the body length) and are shown in Fig. 19 as a function of the angle of attack. The data are very scattered because of small values for the force measurements and therefore the low signal-to-noise ratio. The minimum drag coefficient C_{Df} was estimated to be approximately 0.6 on the basis of the cross-sectional area of the body. This value is smaller than those estimated by Azuma and Watanabe (1988) and larger than those measured by May (1991) at the same Reynolds number.

Conclusions

The aerodynamic characteristics of the wings and body of a dragonfly and of artificial wing models were studied using two types of wind-tunnel tests and free-flight tests using gliders made from dragonfly wings. The wing models were made to examine the effects of the thickness, camber, surface roughness and leading-edge sharpness on the lift curve slope, maximum lift coefficient, minimum drag coefficient and the lift-to-drag ratio. The results from the three experimental methods used in

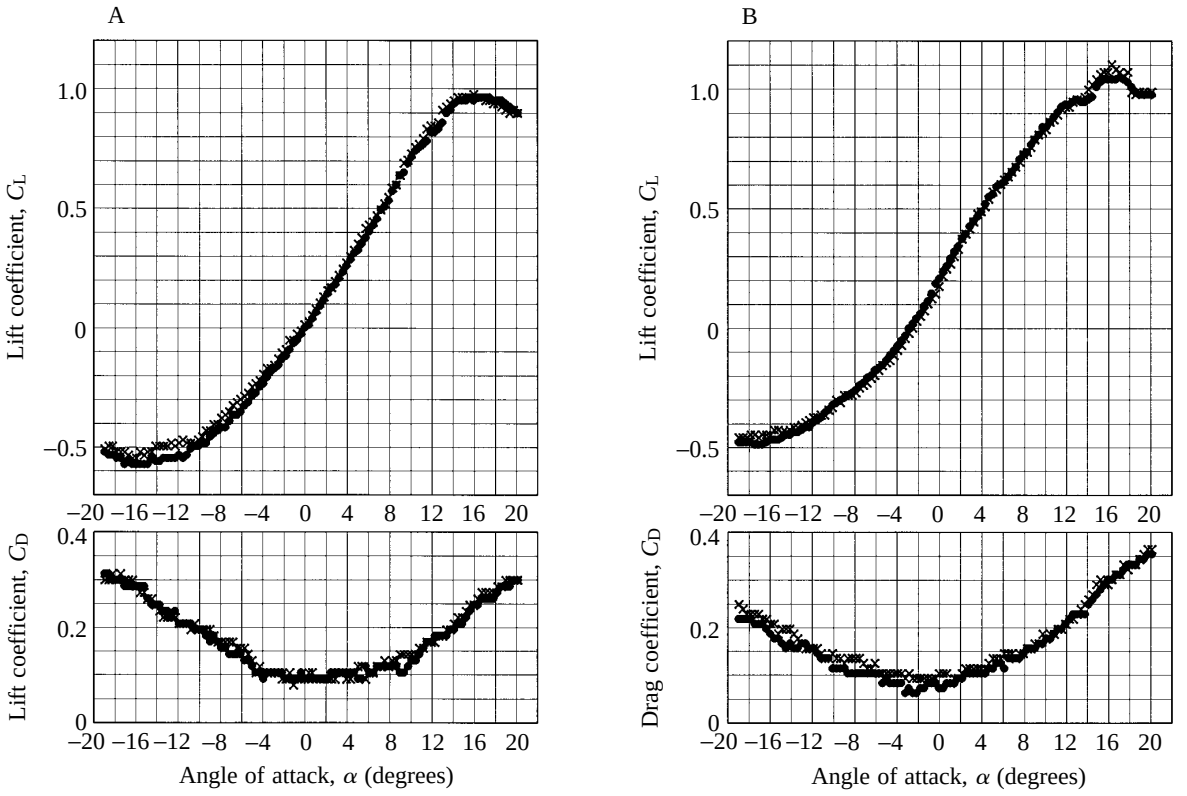

Fig. 16. Aerodynamic characteristics of the modified dragonfly wing shown in Fig. 15B. The wing pair was from dragonfly B in Table 1. Circles indicate results from tests with $\dot{\alpha}>0$, where $\dot{\alpha}$ is the rate of change of the angle of attack. Crosses are for $\dot{\alpha}<0$. (A) C_L (upper panel) and C_D (lower panel) *versus* α for the forewing (AR =5.9). (B) Results for the hindwing (AR =4.5).

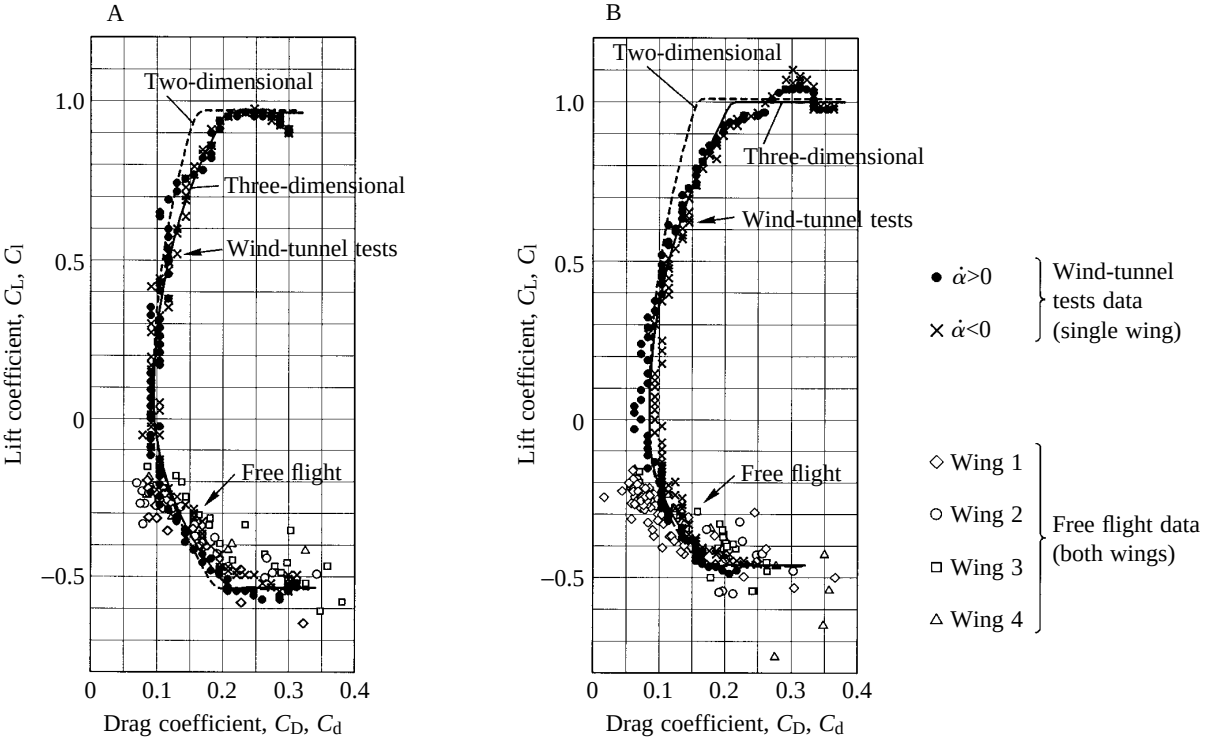

Fig. 17. Polar curves for dragonfly wings. The different symbols indicate different dragonfly wings tested either in the wind-tunnel or in free (gliding) flight. The solid curves represent the glide polar for the data obtained for the three-dimensional wings. The dashed lines are the polar curves calculated from the experimental data for a two-dimensional wing using the local circulation method (LCM). (A) Forewing; (B) hindwing.

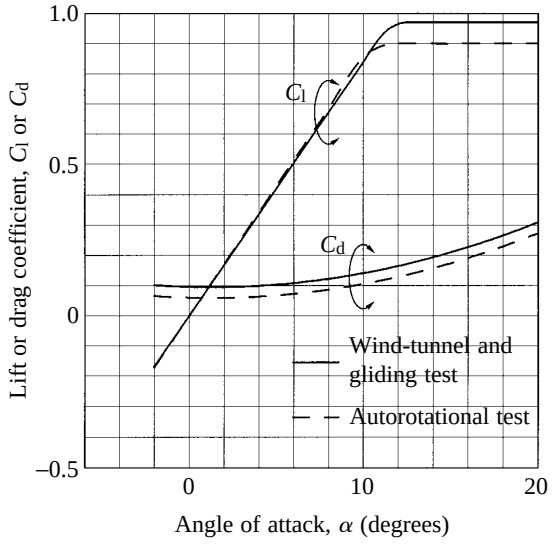

Fig. 18. Two-dimensional aerofoil characteristics of the forewing of a dragonfly. The solid curves are calculated from three-dimensional data obtained in the wind-tunnel and from gliding tests (see text) using the local circulation method (LCM). The broken lines are calculated from data obtained in the autorotational tests (see text) using the LCM.

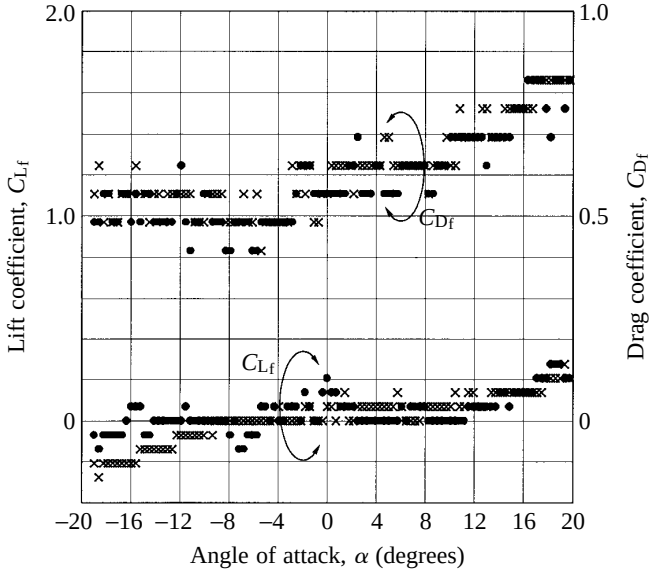

Fig. 19. The aerodynamic characteristics of the body of dragonfly A in Table 1. Filled circles represent values for which the rate of change of the angle of attack ($\dot{\alpha}$) during experiments was greater than 0, crosses represent $\dot{\alpha}<0$. $Re=2.4\times10^4$.

this study showed excellent agreement, giving a high level of confidence in the data.

It has been made clear from the wind-tunnel tests using the model wings that the surface texture or the roughness of the wings will result in an increase in the maximum lift coefficient $C_{L,max}$, the maximum lift-to-drag ratio $(L/D)_{max}$ and the lift coefficient at $(L/D)_{max}$, $C_{L,(L/D)max}$. These characteristics will be favourable for the flight performance of the dragonfly because the polar curve of real dragonflies will be shifted towards higher lift as well as higher drag than the polar curve of the wings alone as a result of the amount of body drag. It is supposed that the dragonfly wing will have been adapted to produce an optimal flight performance.

The paper was presented at the Society for Experimental Biology Symposium, Biological Fluid Dynamics, University of Leeds, UK, held on 4–9 July, 1994.

List of symbols

a	lift slope
AR	aspect ratio ($=b^2/S$)
b	wing span
C_D	drag coefficient of three-dimensional wing ($=D/0.5\rho V^2S$)
C_{D_0}	minimum drag coefficient of three-dimensional wing
C_{Df}	drag coefficient of the body based on its cross-sectional area
C_d	drag coefficient of two-dimensional wing ($=d/0.5\rho V^2c$)
C_{d_0}	minimum drag coefficient of two-dimensional wing
$C_{d,\alpha}$, C_{d,α^2}	drag derivatives of two-dimensional wing
C_L	lift coefficient of three-dimensional wing ($=L/0.5\rho V^2S$)
C_{Lf}	lift coefficient of the body based on its cross-sectional area
$C_{L,max}$	maximum lift coefficient of three-dimensional wing
$C_{L,(L/D)max}$	lift coefficient at the maximum lift-to-drag ratio
C_l	lift coefficient of two-dimensional wing ($=l/0.5\rho V^2c$)
$C_{l,max}$	maximum lift coefficient of two-dimensional wing
C_M	moment coefficient of three-dimensional wing ($=M/0.5\rho V^2Sc$)
c	chord length
D	drag of three-dimensional wing
d	diameter
L	lift of three-dimensional wing
$(L/D)_{max}$	maximum lift-to-drag ratio
l_1, l_2	arm lengths of acting point of forces
l_b	body length
m_b	body mass
m_w	wing mass
M	moment of three-dimensional wing
n	frequency
P_a, P_b, P_c	forces acting on load cells
Re	Reynolds number
S	wing area
S_c	maximal cross-sectional area of the body
S_f	wing area
S_s	area of the settling chamber of the wind-tunnel

S_t	area of the test section of the wind-tunnel
St	Strouhal number (=nd/U)
t	thickness
u	speed of turbulent component of the flow velocity
U	wind speed or flow speed (flight speed plus beating speed)
V	flight speed
α	angle of attack
$\alpha_{Cl=0}$	zero lift angle
β_0	coning angle
γ	gliding angle
ν	kinematic viscosity
ρ	air density
θ	feathering angle
Ω	rotational speed

References

ANDERSON, R. R. (1933). *Charts for Determining the Pitching Moment of Tapered Wings with Sweepback and Twist*. NACA TN 483.

ANDERSON, R. R. (1936). *Determination of the Characteristics of Tapered Wings*. NACA Report 572.

AZUMA, A. (1992). *The Biokinetics of Flying and Swimming*. Tokyo: Springer-Verlag.

AZUMA, A. AND OKUNO, Y. (1987). Flight of samara, *Alsomitra macrocarpa*. *J. theor. Biol.* **129**, 263–274.

AZUMA, A. AND WATANABE, T. (1988). Flight performance of a dragonfly. *J. exp. Biol.* **137**, 221–252.

AZUMA, A. AND YASUDA, K. (1989). Flight performance of rotary seeds. *J. theor. Biol.* **138**, 23–54.

BISPLINGHOFF, R. L., ASHLEY, H. AND HALFMAN, R. L. (1957). *Aeroelasticity*. Reading, MA: Addison-Wesley.

HOERNER, S. F. (1965). *Fluid Dynamic Drag*. 148 Busteed Drive, Midland Park, NJ: Dr Ing. S. F. Hoerner.

MAY, M. L. (1991). Dragonfly flight: power requirements at high speed and acceleration. *J. exp. Biol.* **158**, 325–341.

NEWMAN, B. G., SAVAGE, S. B. AND SCHOUELLA, D. (1977). Model tests of a wing section of an *Aeschna* dragonfly. *Scale Effects in Animal Locomotion* (ed. T. J. Pedley), pp. 445–477. London: Academic Press.

PANKHURST, R. C. AND HOLDER, D. W. (1952). *Wind-tunnel Technique*. London: Pitman & Sons, Ltd.

POPE, A. AND HARPER, J. J. (1966). *Low-speed Wind Tunnel Testing*. New York: John Wiley & Sons.

ROSHKO, A. (1960). Experiments on the flow past a circular cylinder at very high Reynolds numbers. *J. Fluid Mech.* **10**, 345–356.

WEIS-FOGH, T. (1956). Biology and physics of locust flight. II. Flight performance of the desert locust (*Schistocerca gregaria*). *Phil. Trans. R. Soc. Lond. B* **239**, 459–510.